MULTI-COMPONENT TIME-LAPSE SEISMIC: ON SATURATION-PRESSURE DISCRIMINATION AND STATISTICAL DETECTABILITY OF FLUID FLOW

A. SHAHIN, P.L. STOFFA, R.H. TATHAM and D. SAVA

Jackson School of Geosciences, The University of Texas at Austin, Austin, TX 78713, U.S.A.

(Received April 29, 2010; revised version accepted September 8, 2011)

ABSTRACT

Shahin, A., Stoffa, P.L., Tatham, R.H. and Sava, D., 2011. Multi-component time-lapse seismic: on saturation-pressure discrimination and statistical detectability of fluid flow. *Journal of Seismic Exploration*, 20: 357-378.

We evaluate the production-induced time-lapse response of three sandstone reservoirs corresponding to three rock physics models spanning a full range of common degrees of consolidation. For a range of water saturation and pore pressure, we compute multi-component (MC) seismic, i.e., conventional P-P, converted P-SV, and pure shear SH-SH, traveltimes through and reflection coefficients (RCs) at top of the sandstone reservoir embedded in a background shale.

Then, we compute changes in traveltimes and reflection coefficients with respect to a reference traveltime and RC calculated at reference saturation and pressure conditions. We plot changes in RCs versus changes in traveltimes. The corresponding time-lapse cross-plot shows interesting patterns for saturation and pressure changes and has the potential for quantitatively discriminating pressure and saturation changes.

Next, we deploy a statistical method to determine the efficacy of MC seismic in detecting production-induced time-lapse changes. The significant and representative data in time-lapse cross-plot allow one to statistically analyze the detectability of a known scenario of saturation and pressure changes using MC seismic attributes. Applying different thresholds for traveltimes and RCs, we construct single and joint probability detectors that help to compare the likelihood of detection of a known change in dynamic reservoir properties using different component of the seismic data. Our analysis demonstrates that seismically detection of the changes in fluid saturation and pressure is significantly limited for a consolidated sandstone reservoirs. However, the detection is plausible for poorly to medium consolidated reservoirs in the presence of realistic seismic noise levels. In these cases, conventional P-P seismic data is dominant in amplitude change compared to converted

0963-0651/11/$5.00

P-SV and pure SH-SH seismic data. P-P data reflects changes in both fluid saturation and pore pressure. However, the main effect of P-P data is the saturation component than pressure. SH-SH seismic data capture most the pressure information using traveltimes of pre-stack data. P-SV seismic data is the weakest detector of changes in time-lapse amplitude, but its traveltime shows an intermediate detectability between P-P and SH-SH seismic data for changes in both fluid saturation and pressure.

KEY WORDS: seismic, 4D, multi-component, saturation, pressure, probability, detection.

INTRODUCTION

Seismic reflection data have been used to estimate lithology and fluid of subsurface rocks. Various seismic attributes can be extracted from seismic volumes in order to qualitatively, semi-quantitatively, and quantitatively perform seismic litho-fluid facies classifications. Pattern recognition techniques, multivariate statistical methods, Bayesian classification, and neural networks have been utilized to map litho-fluid facies from seismic data. In most cases, authors have addressed cross-plotting of seismic attributes to classify seismic volumes into distinct litho-cubes. For example, Fournier et al. (2002) used supervised and unsupervised statistical pattern recognition techniques to classify seismic volumes via cross-plotting of seismic attributes computed from seismic traces within reservoir intervals. Inverted seismic parameters, e.g., acoustic (AI) and shear impedances (SI), extracted from pre-stack seismic data can also be used to classify seismic volumes. In doing so, cross-plots of the inverted parameters are made. Similarly, elastic parameters derived from well log information are commonly cross-plotted and color-coded with other discriminatory well log-derived data such as shale fraction and porosity. The well log analysis allows one to distinguish lithology and fluid classes which will guide the classification of the inverted seismic attributes in crossplot domains. Finally, lithology and fluid clusters are back-projected from cross-plot domains to seismic volumes (Avseth et al., 2005).

The above summary is a review of the current state-of-the-art technology in classifying seismic volumes into fluid and rock facies. In this paper, we first investigate the problem of classifying time-lapse signals to associated changes in saturation and pressure due to a waterflooding scenario. Next, we deploy a statistical method to determine the efficacy of MC seismic in detecting production-induced time-lapse changes. Afterward we present a summary of different approaches currently employed in the petroleum industry to investigate time-lapse data and then we focus on the crossplotting of time-lapse signals, which is the main focus of this paper.

Time-lapse seismic data consist of two or more repeated seismic surveys recorded at different calendar times over a depleting reservoir in primary, secondary, or tertiary recovery phases. Seismic reservoir monitoring of a

waterflooded reservoir is a challenging problem. Detecting small changes in seismic traveltimes and RCs due to changes in dynamic reservoir properties, i.e. water saturation and pore pressure may be the key to success. Seismic waveform data contain two types of information: amplitude and traveltime. Amplitude is the convolution of RC series and a wavelet. RC responds to interface properties, i.e., contrasts in P- and S-wave velocities and contrast in density between adjacent layers. On the other hand, seismic traveltime responds to interval properties, i.e., absolute values of P&S-wave velocities in the desired subsurface interval. These seismic attributes, RCs and traveltimes, are complicated functions of the elastic parameters of rocks. Elastic parameters are also related to the properties of the solid and fluid parts of the rocks, porosity, clay content, pressure, saturation, etc. through a set of complex and nonlinear equations defining rock physics models, e.g., Hertz-Mindlin (Mindlin, 1949) and Gassmann (1951) theories. Consequently, making any judgment about dynamic reservoir properties using seismic attributes is challenging and dependent on the rock physics model employed.

Depending on ambiguities in the description of the reservoir architecture, quality of the seismic data, and economic consideration of the field under study, seismic time-lapse interpretation can be performed at three different levels.

The first approach is the qualitative interpretation of changes in seismic observations, amplitude, traveltime, and an interpretive association of the changes in the seismic attributes to changes in reservoir parameters, e.g., porosity, saturation, pressure, temperature, etc. The qualitative interpretation of time-lapse seismic data has been addressed by numerous workers, e.g. Cooper et al. (1999), Lumley et al. (1999), Marsh et al. (2001), Rutledal et al. (2002), Behrens et al. (2002), and various papers in Parker et al. (2003). The primary objective of this type of analysis is to indentify flood fronts, preferential pathways, thief zones, and flow barriers, by-passed pay zones and infill drilling targets. Most of the authors mentioned that these objectives have been achieved and time-lapse seismic data have a positive impact on field development.

The second and more advanced methodology is to semi-quantitatively or quantitatively interpret or invert changes in seismic observations to changes in fluid saturation and pressure. This approach is the main topic of this paper and is discussed in detail below.

The third and most recent application of time-lapse seismic is referred to as seismic reservoir history matching, 4D history matching, or reservoir history matching constrained by time-lapse seismic data. This currently evolving technology is a multi-disciplinary approach to integrate well logs, core analyses, production data, and time-lapse seismic reflectivity data aimed at updating a reservoir model. Reservoir modeling and simulation, petro-elastic rock and fluid modeling, seismic wave propagation modeling, and joint inversion of measured

seismic and production data, are some of disciplines involved in this technique. Several case studies, e.g., Walker et al. (2006) in the Andrew, Valhall, and Harding fields in the North Sea, have demonstrated that joint history matching of seismic and production data leads to a positive impact on the quality of the estimated reservoir parameters relative to estimates obtained from production history matching alone. This is due to the additional spatial knowledge contained in time-lapse seismic data. The main focus of this paper is to separate the changes in fluid saturation and pressure using changes in seismic attributes due to time-dependent reservoir production. Now, we focus on the main topic of this paper to quantitatively associate the changes in time-lapse seismic observations, i.e. traveltime and amplitude, to the changes in fluid saturation and pressure. This approach has been addressed by several authors in the literature, so we briefly review the previous works.

Some workers make use of inverted elastic parameters, e.g., AI and SI changes, to indirectly estimate pressure and saturation changes via cross-plotting methods. To summarize, Tura and Lumley (1999) estimated changes in saturation and pressure via cross-plotting of inverted AI and SI changes. Cole et al. (2002) proposed a grid search method to estimate pressure and saturation by forward modeling of rock and fluid physics. Lumley et al. (2003) proposed a 4D seismic cross-plot inversion method using a coordinate transformation and calibration with well data to simultaneously estimate pressure and saturation changes. Andersen et al. (2006) and Andersen et al. (2009) proposed a dual cross-plotting technology for the seismic facies classification problem. First, a crossplot of the inverted seismic attributes, i.e., [V_P/V_S vs. AI], for the base survey is created and lithofacies are then classified accordingly. Second, time-lapse effects are classified via cross-plotting of 4D seismic attributes, i.e., [$\Delta(V_P/V_S)$ vs. ΔAI], where Δ denotes a change in any parameter due to production between base and monitor surveys. From 4D crossplots, one can classify the seismic volume into different subsets associated with scenarios of changes in pore pressure and/or saturation. Finally, the lithofacies and 4D classes are combined via dual classification to reveal pure and combined 4D effects in pay zones.

Some techniques have been proposed to directly invert or transfer time-lapse seismic data to fluid saturation and pressure changes. For example, Landrø (2001) and Landrø et al. (2003) directly inverted time-lapse seismic data for fluid saturation and pressure changes based on an approximate rock physics model and a linearized form of reflection coefficients. Other authors (e.g., Angelov, 2004) made improvements based on Landrø's method. Veire et al. (2006) presented a stochastic inversion method to discriminate pressure and saturation changes directly from P-P time-lapse AVO data. MacBeth et al. (2006) developed a first order linear formula relating changes in any pair of seismic attributes to changes in pressure and saturation.

As our first contribution to this work (Shahin et al., 2009), we introduce a methodology to make a MC seismic time-lapse crossplot. Then, we will show how one can directly transfer changes in MC seismic traveltimes and reflection coefficients to changes in fluid saturation and pressure. In this method, there is no inversion involved. No assumption for rock physics is necessary. However, the methodology is only appropriate for single layer reservoirs. We further assume that water injection into a black oil reservoir is an isothermal process. In addition, we assume that changes in fluid saturation and pore pressure do not cause any mechanical compaction on the reservoir or the background shale.

Lumley et al. (1997) presented a method for assessing the technical risk of a P-P 4D seismic reservoir monitoring project in any production, reservoir and field conditions. They evaluated important reservoir and seismic parameters and assigned scores based on their experiences from various 4D seismic projects worldwide. After assigning scores, each individual reservoir will be a candidate for a future 4D project if it passes the 60% threshold of both reservoir and seismic scores of the ideal case. The method is fast and tested for different geographical fields. However, it is mainly based on experience and leads to a deterministic answer based on the 60% rule. In addition, it is only for conventional P-P 4D projects, and not for P-SV and SH-SH surveys.

As a second contribution to this research, we develop a statistical detectability criterion using time-lapse cross-plots. This approach is able to estimate the likelihood of detecting a known production scenario using MC 4D seismic surveys. It can be easily tested for different reservoir types under various production conditions and leads to a probabilistic answer based on the quality of the available seismic data.

METHODOLOGY

In general, seismic reservoir monitoring results in a better understanding of flood fronts, preferential fluid migration, and flow barriers, followed by more effective reservoir management. This task is often applicable after determining the static reservoir properties in the reservoir characterization stage. In other words, obtaining a reasonable static model including porosity, permeability, and lithology variations within the reservoir is an essential step before implementing seismic time-lapse analyses.

Assuming a well-defined initial static model, reservoir simulator can be run for a desirable production scenario. Then, the range of changes in dynamic reservoir properties, e.g., water saturation and pore pressure in a waterflooding scenario, can be recorded between two calendar times. Using the average static reservoir properties, i.e., constant values of porosity, reservoir thickness, clay content, etc., a simulated reservoir segment is generated. The simulated segment

is a representative segment of the reservoir containing the average properties of the actual reservoir. Our analysis is applied on this segment, but the same procedure can be implemented on different simulated segments, where their reservoir properties are perturbed properties of the representative segment.

The representative segment is embedded in background shale simulating the surrounding sedimentary rocks. Assigning the same scenarios of changes in saturation and pressure as the actual reservoir, one can calculate P- and S-wave velocities and density of the reservoir segment using Gassmann's theory and a stress-sensitive rock physics model, e.g., modified Hashin-Strikman lower bound, (Dvorkin and Nur, 1996), calibrated with pressure-dependent core measurements. Next, we calculate MC seismic traveltimes within the reservoir either numerically, using ray tracing, or analytically assuming straight rays. In addition, we compute MC seismic RCs at the reservoir top. Then, we subtract an initial traveltime and RC, calculated for the reference pressure and saturation, from the above-calculated traveltimes and RCs, respectively. Then we plot changes in RCs at the top of the reservoir versus changes in traveltimes through the reservoir. The corresponding time-lapse cross-plot shows interesting patterns for saturation and pressure changes and has the potential for quantitatively discriminating pressure and saturation changes.

In addition, the data in time-lapse cross-plot allow one to statistically analyze the detectability of a known scenario of saturation and pressure changes using MC seismic attributes. The single and joint Cumulative Distribution Function (CDF) for changes in MC seismic traveltimes and RCs provides a convenient way to obtain specific probabilities at desirable ranges of time-lapse attributes. Applying different thresholds for detectability of traveltimes and RCs, we construct single and joint probability detectors, called SPD and JPD, respectively. These detectors are effective tools that determine the likelihood of detecting the desirable ranges of changes in traveltimes and RCs for known changes in fluid saturation and pore pressure.

Finally, instructive forward modeling of this type for actual reservoirs will help to determine the detectability of dynamic reservoir properties using MC time-lapse seismic attributes. That is, repeating the above procedure for various simulated segments with different porosities, thicknesses, and clay contents, will give insight into the classification of various reservoir types or different parts of a laterally varying reservoir from a detectability point of view.

SYNTHETIC EXAMPLE

Three synthetic sandstone reservoir units embedded in background shale are considered to show the efficacy of the methodology presented in this paper. Table 1 summarizes the characteristics of these reservoir units, A, B, and C.

Table 1. Characteristics of three synthetic reservoir units used in this study.

	Reservoir A	**Reservoir B**	**Reservoir C**
Degrees of consolidation	Consolidated sandstone	Medium-consolidated sandstone	Poorly-consolidated sandstone
Rock physics model	Stiff sand model or modifies Hashin-Strikman upper bound (Gal et al. 1998)	Average of upper and lower bound for reservoir A and C	Modifies Hashin-Strikman lower bound (Dvorkin and Nur 1996)
Porosity (%)	10	20	30
Critical porosity (%)	40	40	40
Depth (m)	3000	2200	1500
Thickness (m)	100	100	100
Temperature(^{0}C)	100	75	55
Salinity (PPM)	70000	70000	70000
Clay content (%)	20	20	20
Average contact number	6	6	6
Initial pore pressure (psi)	5000	4000	3000
Overburden pressure (psi)	10000	7000	5000
Effective pressure (psi)	5000	3000	2000
Change in initial pore pressure (psi)	-1500 to 1500	-1200 to 1200	-900 to 900
Initial water saturation	0.50	0.50	0.50
Change in initial water saturation	-0.35 to 0.35	-0.35 to 0.35	-0.35 to 0.35

Table 2. Density and elastic properties of minerals associated with the synthetic reservoirs.

Constituents	Density (g/cm^3)	Bulk modulus (GPa)	Shear modulus (GPa)	P-wave velocity (km/s)	S-wave velocity (km/s)
Quartz	2.65	37.0	44.0	6.008	4.0748
Clay	2.55	25.0	9.0	3.8092	1.8787

The reservoirs are composed of 80% quartz (Mavko et al., 2009) and 20% clay (Han, 1986). Table 2 shows the elastic properties of the minerals in the reservoirs.

Three reservoir units are located at different depths based on degrees of consolidations and the corresponding rock physics models are selected accordingly. Fig. 1 displays the adopted rock physics models for this study. Reservoir A is consistent with the modified upper Hashin-Strikman (MUHS) bounds (continuous and dashed black lines for P- and S-wave velocities versus porosity, respectively) with 10% porosity. Reservoir C is consistent with the modified lower Hashin-Strikman (MLHS) bounds (continuous and dashed blue

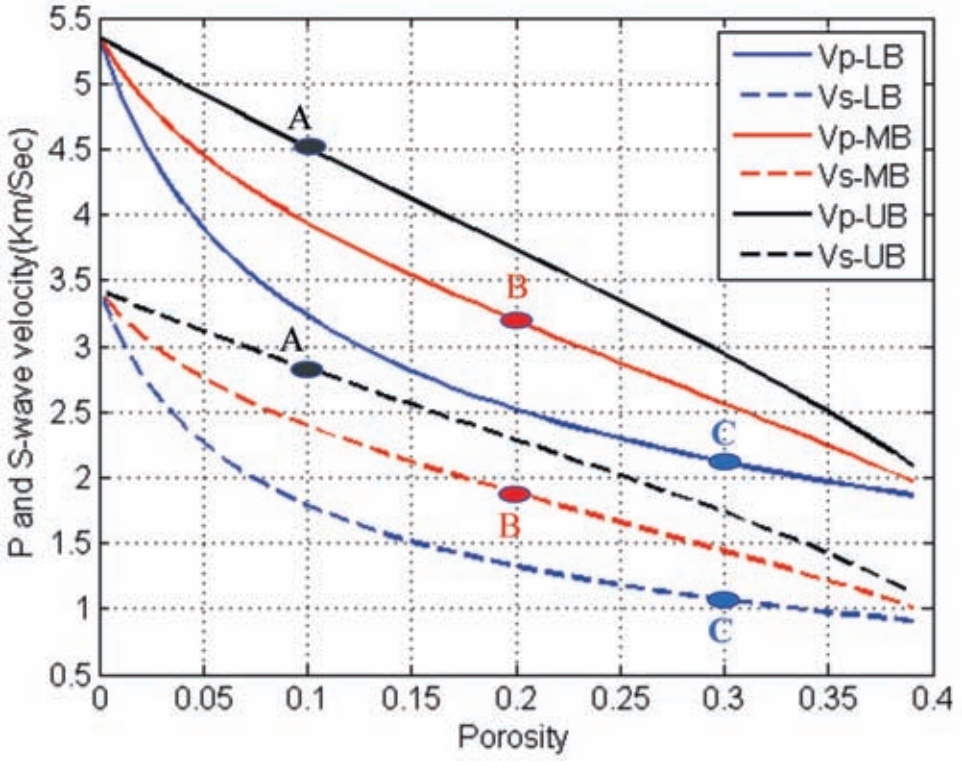

Fig. 1. Rock physics models (P-wave and S-wave velocities versus porosity) adopted for this study. Continuous and dashed black lines are modified Hashin-Strikman upper bounds (Stiff sand model, Gal et al., 1998) for P- and S-wave velocities, respectively. Reservoir A is located on these bounds with 10% porosity. Continuous and dashed blue lines are modified Hashin-Strikman lower bounds (Dvorkin and Nur, 1996) for P&S-wave velocities, respectively. Reservoir C is located on these bounds with 30% porosity. Continuous and dashed red lines are the average of upper (UB) and lower (LB) bounds and called middle bounds (MB). Reservoir B is positioned on these bounds with 20% porosity.

lines for P- and S-wave velocities versus porosity, respectively) with 30% porosity. Reservoir B with 20% porosity is positioned on velocity vs. porosity curves averaging the MUHS and MLHS bounds (continuous and dashed red lines for P- and S-wave velocities, respectively). With these models, we span a wide range of sandstone reservoirs worldwide and evaluate the corresponding production-induced time-lapse signal. Porosity is depth dependent and reduces with increasing depth. Reservoir temperature, initial pore pressure, and overburden pressure are also depth dependent. A constant reservoir thickness of 100 meters is considered for all three reservoirs. Fluid properties are extracted from pressure, volume, temperature (PVT) data (Killough, 1995) and then transformed to seismic elastic parameters using Batzle and Wang's (1992) empirical correlations (Fig. 2). Discontinuity on the oil P-wave velocity at 2000 psi is related to the bubble point pressure.

At initial production, we assume the reservoir is uniformly saturated with 50% brine (connate water) and 50% light oil. This will be the reference water saturation to calculate time-lapse attributes. Initial pore pressures differ for the three reservoirs depending on the depth at which each reservoir is located. A known scenario of changes in water saturation, −70% to +70% of the initial water saturation, and changes in pore pressure, −30% to +30% of the initial

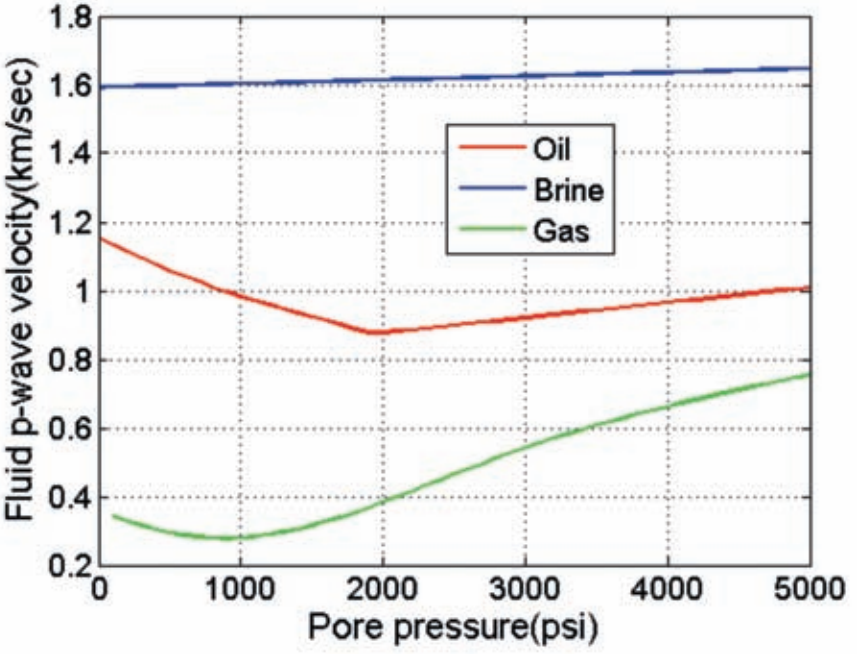

Fig. 2. Seismic P-wave velocity for the reservoir fluids. Batzle-Wang 1992 empirical relationships have been used to transform PVT properties of oil-gas-water. Note that bubble point pressure is 2000 psi.

pore pressure, are intended to simulate a water-flooded black oil reservoir. Note that percentages of changes in pore pressure are relative values, i.e., the absolute values differ for pore pressure depending on initial pore pressure (Table 1). The assigned ranges of pore pressure variations are always above the bubble point pressure; consequently, no gas is produced within the reservoirs and light oil and brine water are the only liquid phases.

We use Biot-Gassmann's theory (Gassmann, 1951; Biot, 1956) to predict how seismic velocities depend on pore fluids. Stress-sensitive rock physics models are implemented to predict the pressure effect on seismic velocities. Fig. 3 illustrates the effects of water saturation (first panel) and pore pressure (second panel) on density and elastic parameters of reservoir rocks. The first panel shows the relative and normalized values of changes in density and velocities due to changes in water saturation. It is computed at the constant effective pressure associated with each reservoir. It is clear that the lower bound is most sensitive to water saturation, the middle bound has the second rank, and the upper bound is the least sensitive one. Since water bulk modulus and density are greater than those of oil, P-wave velocity (V_P) and density (Rho) increase when water saturation goes up, i.e., oil is replaced with water. In contrast, S-wave velocity (V_S) decreases with increasing water saturation. This is only a density effect because the shear modulus of the rock is unaffected by fluids based on the Bio-Gassmann theory. The second panel shows the relative and normalized values of changes in seismic velocities due to changes in pore pressure. It is computed at constant initial water saturation associated with each reservoir. Similar to the first panel, lower bound is most sensitive to pore pressure, middle bound has the second rank, and upper bound is the least sensitive one. Both V_P and V_S decrease with increasing pore pressure. However, V_S is more sensitive to pore pressure than V_P. Density is almost insensitive to pore pressure variations (not shown here). The interesting asymmetric trend demonstrates that elastic parameters are more sensitive to pore pressure increase than decrease. This suggests that in a time-lapse seismic study, pore pressure detection should be easier near the injector wells than producers.

Using all of the above reservoir properties, three reservoir units are generated and embedded in the background shale at different depths. The elastic properties of shale, i.e., density of 2.35 g/cc, P-wave velocity of 3 km/s, and S-wave velocity of 1.7 km/s, are extracted from Blangy (1994). MC seismic traveltimes (T_{PP}, T_{PS}, and T_{SS}) within the reservoir and RCs (RC_{PP}, RC_{PS}, and RC_{SS}) at reservoir top are then calculated for the same percentage of changes in water saturation and pore pressure and for incident angles up to 20 degrees (Sub indices of pp, ps, and ss indicate conventional P-P, converted P-SV, and pure SH-SH seismic reflectivity data and will be used here after in the text and figures). Then, MC seismic traveltimes and RCs are subtracted from initial traveltimes and RCs computed at the reference water saturation and pore pressure for each individual reservoir.

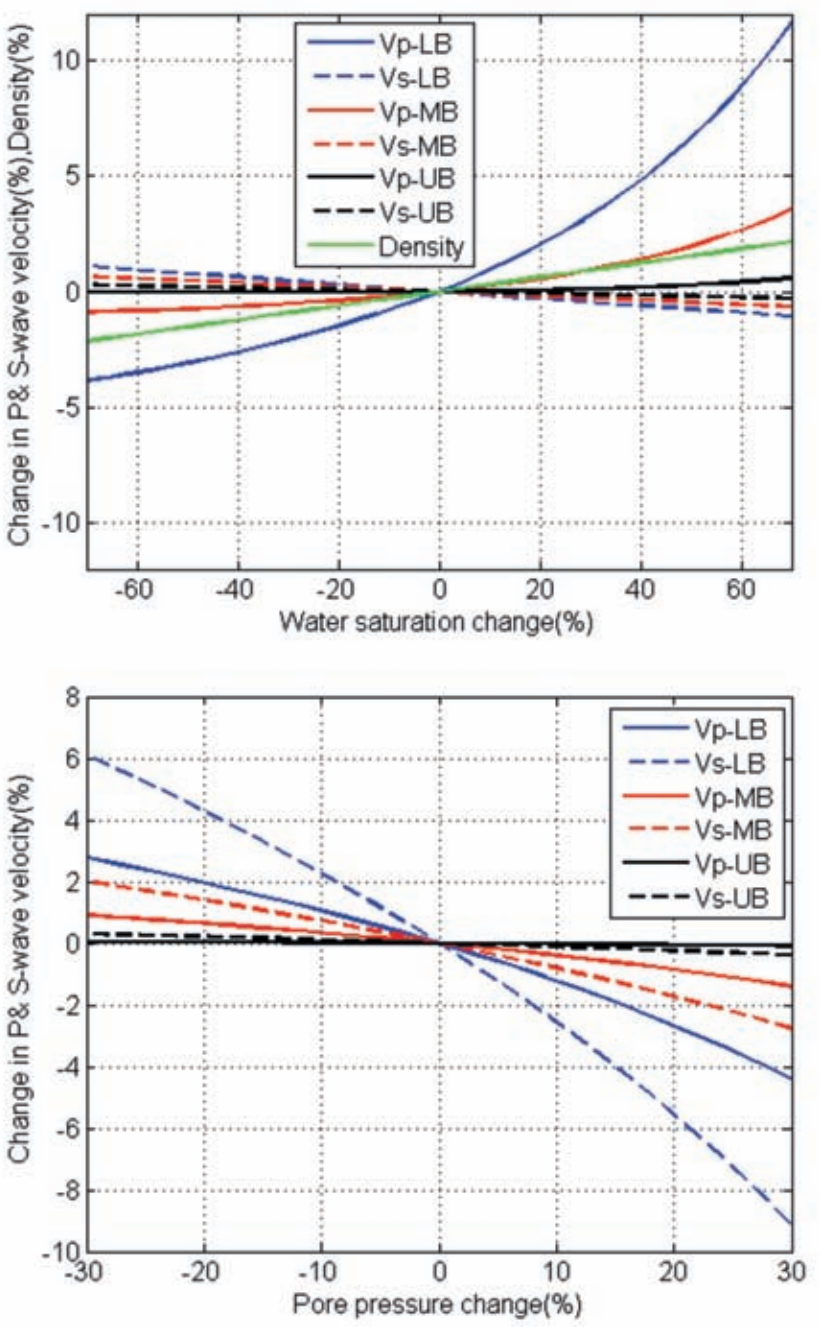

Fig. 3. Effects of water saturation (upper panel) and pore pressure (lower panel) on density, P- and S-wave velocities of the reservoir rocks. Continuous and dashed lines indicate P- and S-wave velocities, respectively. Upper bounds (UB) are shown in black, lower bounds (LB) in blue, and middle bounds (MB) in red.

Figs. 4, 5, and 6 display the joint effect of changes in water saturation and pore pressure on MC seismic traveltimes and RCs for reservoir A, B, and C, respectively. The first row of each figure show the changes in traveltime and the second row show the corresponding changes in RCs. When comparing changes in traveltimes for reservoirs A, B, and C, one can state that the ranges of -10 to $+20$ millisecond (ms) for reservoir C are easily detectable, ranges of -4 to $+3$ ms for reservoir B are barely detectable, and ranges of -1 to $+1$ ms for reservoir A are not detectable. The same statement is true for the amplitude of time-lapse signals. A correlation exists between the changes in traveltimes and the associated changes in RCs. That is due to the changes in fluid saturation and pore pressure and this encourage authors to make crossplots of changes in RCs versus changes in traveltimes to explore this correlation in more detail. We also investigate if there is any pattern to estimate and separate the effect of fluid saturation and pore pressure when only MC time-lapse traveltimes and RCs are available.

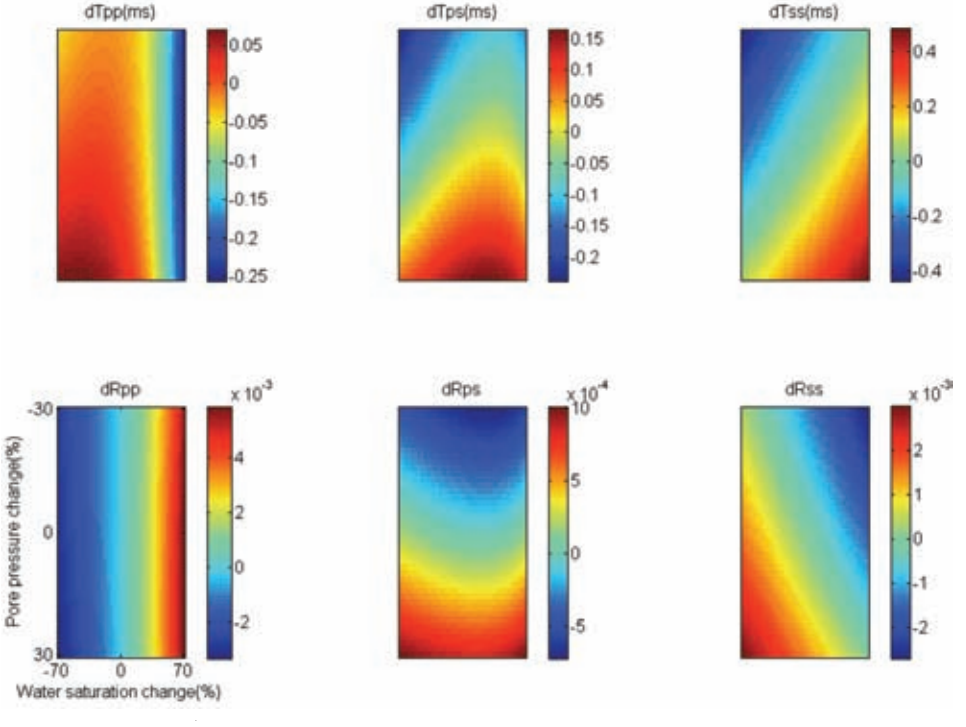

Fig. 4. Reservoir A: Joint effects of changes in water saturation and pore pressure on Multi-Component (MC) seismic traveltimes (first row) and Reflection Coefficients, RCs, (second row). dTpp, dTps, and dTss are the changes in MC traveltimes for conventional P-P, converted P-SV, and pure SH-SH seismic reflectivity data. dRpp, dRps, and dRss indicate the associated changes in MC RCs.

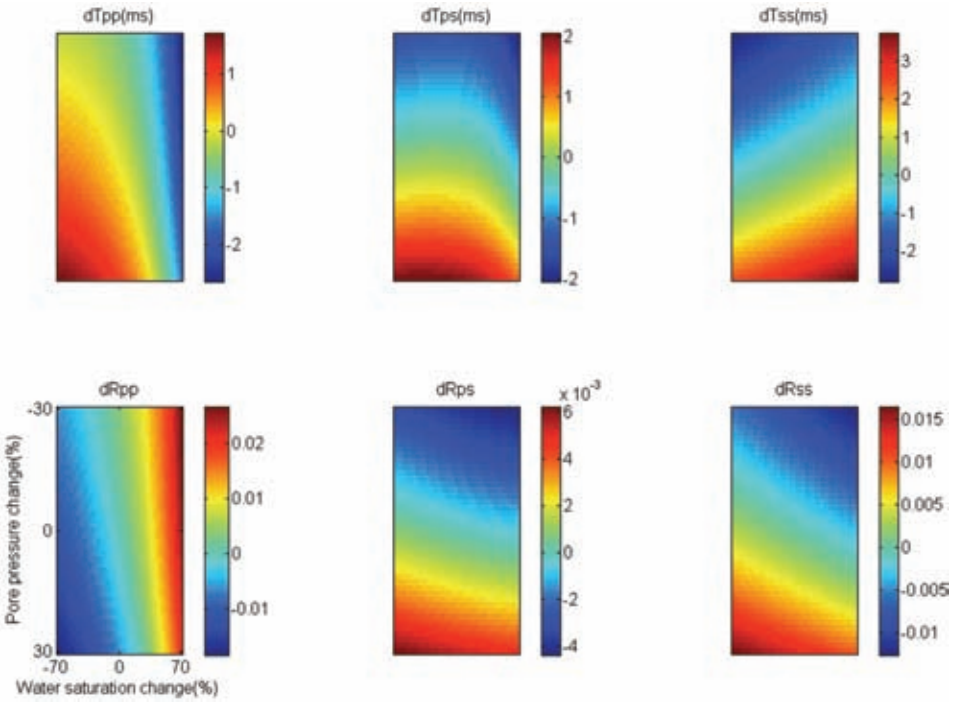

Fig. 5. Reservoir B: Joint effects of changes in water saturation and pore pressure on Multi-Component (MC) seismic traveltimes (first row) and Reflection Coefficients, RCs, (second row). dTpp, dTps, and dTss are the changes in MC traveltimes for conventional P-P, converted P-SV, and pure SH-SH seismic reflectivity data. dRpp, dRps, and dRss indicate the associated changes in MC RCs.

Fig. 7 illustrates scatter plots for pairs of RCs changes versus traveltime changes computed for the reservoir C. The upper panel show a noise-free data set generated with large increment in water saturation and pore pressure changes. Incident angle varies between 0 to 20 degrees. By choosing such geometry, we can see some pattern in RCs and traveltimes. These patterns are associated with enforced patterns in water saturation and pore pressure changes. The origin, i.e., (0, 0), of this cross-plot corresponds to zero change in saturation and pressure. Two trends exist for saturation and pressure of P-P and SH-SH reflectivity data, but P-SV lacks these trends. This is due to fact that P-SV data has one way travel time through the reservoir with P-wave velocity and one way with S-wave velocity. The total traveltime is mainly affected with saturation in one path and with pressure in the other path, so separation is difficult for P-SV data using this kind of crossplotting. From the spread of

points in the traveltime direction, it is evident that the value of traveltime for pressure detection is higher for SH-SH than that of P-P. However, spread of points in the RCs direction indicates that the value of RCs for saturation detection is higher for P-P than that of SH-SH.

One of the applications of time-lapse cross-plots is to quantitatively estimate and discriminate pressure and saturation changes from MC RCs and traveltime changes in a 4D project (upper panel in Fig. 7). The other application is to statistically evaluate the cross-plot and to create criteria for detectability of a known production scenario using MC seismic measurements. To reach this goal, we first generate a set of noisy data set, contaminated with 10% Gaussian random noise, by choosing a small increment in water saturation and pore pressure. The representative data in time-lapse cross-plot (lower panel in Fig. 7) allow one to statistically analyze the detectability of a known scenario of saturation and pressure changes using MC seismic attributes. Next, we construct

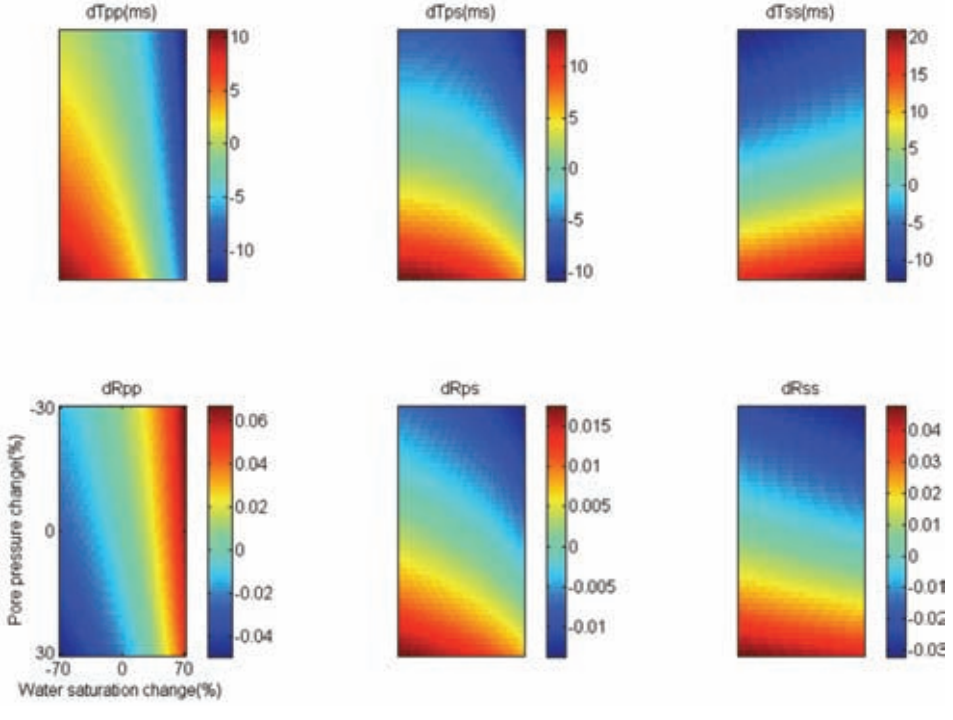

Fig. 6. Reservoir C: Joint effects of changes in water saturation and pore pressure on Multi-Component (MC) seismic traveltimes (first row) and Reflection Coefficients, RCs, (second row). dTpp, dTps, and dTss are the changes in MC traveltimes for conventional P-P, converted P-SV, and pure SH-SH seismic reflectivity data. dRpp, dRps, and dRss indicate the associated changes in MC RCs.

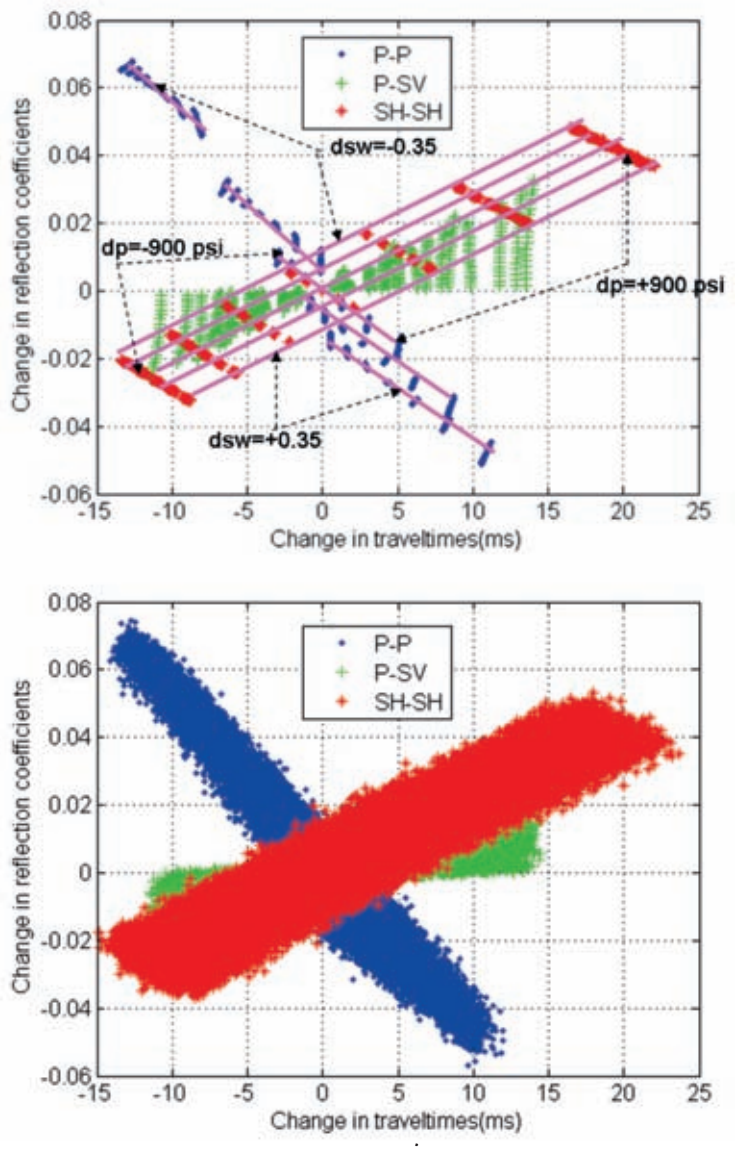

Fig. 7. Cross-plots of changes in RCs versus changes in travel times (ms), for reservoir C. First panel is noise-free data set with large increment in water saturation (ranged from −0.35 to +0.35 by increment of 0.20) and pore pressure (ranged from −900 to +900 by increment of 300 psi). P-P cloud is shown in blue, P-SV in green, and SH-SH in red. Continuous pink lines indicate saturation patterns for changes of −0.35, −0.20, 0.0, +0.20, and +0.35 from bottom to top for P-P and from top to bottom for SH-SH. Black dashed arrows display the extreme values for two end members of −0.35 and +0.35. For pressure patterns, black dashed arrows display the extreme values for two end members of −900 and +900 psi from left to right for SH-SH and from top to bottom for P-P. Note that P-SV data lacks pattern for saturation and pressure. Second panel is contaminated data set with 10% random Gaussian noise and with small increment in water saturation (ranged from −0.35 to +0.35 by increment of 0.01) and pore pressure (ranged from −900 to +900 by increment of 5 psi).

single and joint distributions functions for changes in RCs and traveltimes. Fig. 8 displays the single probability density function (PDF) for the RCs on the left column and for traveltimes on the right column. Three rows in this figure from top to bottom correspond to reservoir A, B, and C, respectively. This figure summarizes the entire information hidden in previous figures and provides a concise and instructive manner to represent time-lapse signals. Fig. 9 shows the joint probability density function (JPDF), the associated marginal single PDFs, the joint cumulative distribution function (JCDF), and the corresponding single CDF of reservoir C and only for P-P seismic data.

Having calculated the single CDF for time-lapse attributes (Fig. 9), the probabilities of detecting certain symmetric ranges of time-lapse seismic attributes can be computed. Fig. 10 illustrates single probability detectors (SPDs) for RCs on the left and for traveltimes on the right column. As an example for application of SPDs, assume that any changes in seismic traveltimes greater than plus minus 5 ms are detectable based on the quality of the seismic data. For reservoir C, using the right lowermost panel of SPDs in Fig. 11, the likelihood of having detectable traveltime for the specific production plan, will

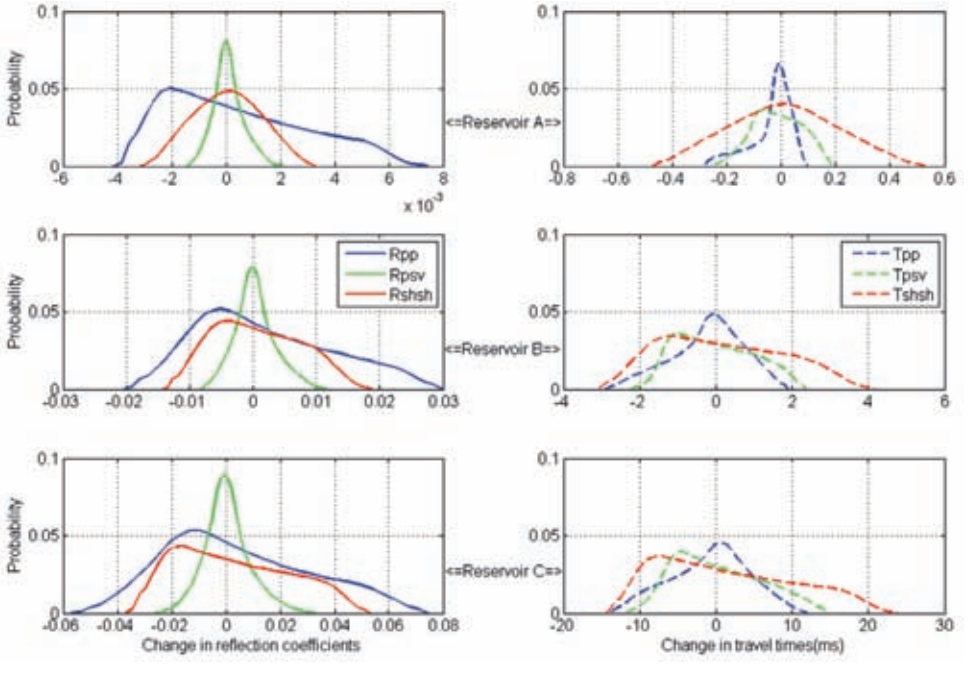

Fig. 8. Single probability density function (PDF) for the RCs on the left column and for traveltimes on the right column. Three rows in this figure from top to bottom correspond to reservoir A, B, and C, respectively.

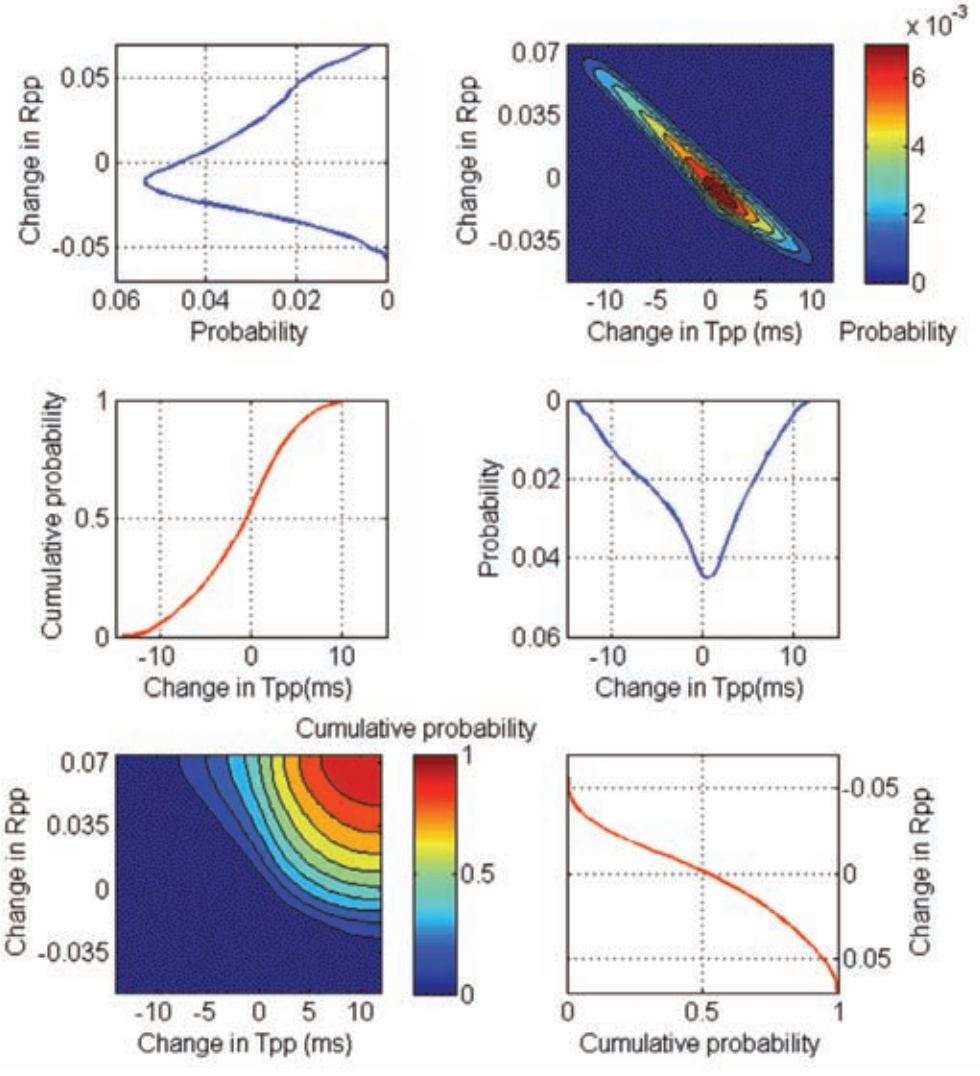

Fig. 9. Joint probability density function (JPDF), the associated marginal single PDFs, the joint cumulative distribution function (JCDF), and the corresponding single CDF of reservoir C and only for P-P seismic data.

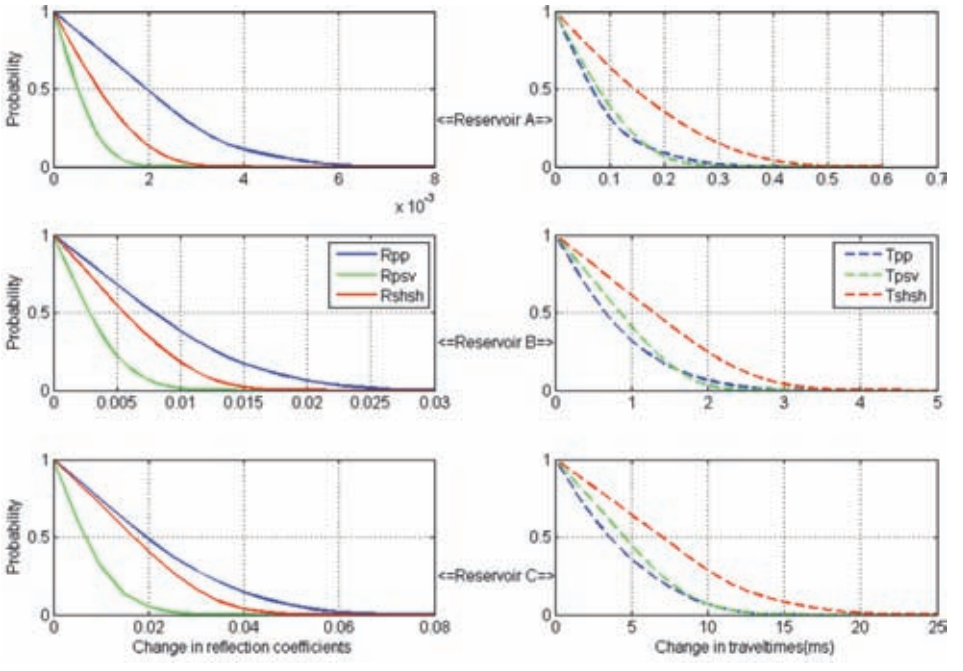

Fig. 10. Single probability detectors (SPDs) for RCs on the left and for traveltimes on the right column. Three rows in this figure from top to bottom correspond to reservoir A, B, and C, respectively.

be 30, 40, and 65 percent, using P-P, P-SV, and SH-SH seismic data, respectively. By comparing SPDs of three reservoirs in Fig. 11, one can determine that under specific conditions set for our reservoirs in this study, time-lapse signals for the reservoir A are not detectable, for reservoir B barely detectable, and for reservoir C more likely detectable.

In Fig. 11, we color-plot the joint probabilities of detecting certain symmetric ranges of time-lapse seismic attributes and called them joint probability detectors (JPDs). Horizontal axes on these plots are the absolute (positive) values of changes in seismic traveltimes. Vertical axes are absolute values of changes in seismic RCs. As an example for application of JPDs, assume that any changes in seismic traveltimes greater than plus minus 5 ms, and any changes in seismic amplitude greater than plus minus 0.01 are detectable. For reservoir C, using the last row of JPDs in Fig. 11, the likelihood

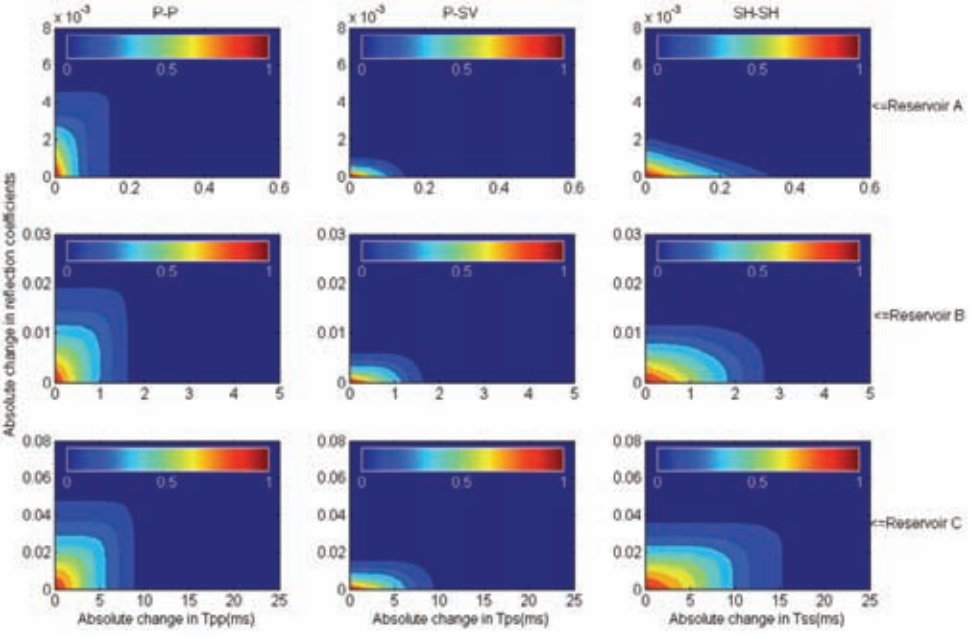

Fig. 11. Joint probability detectors (JPDs) for three synthetic reservoirs. Three rows in this figure from top to bottom correspond to reservoir A, B, and C, respectively. Horizontal axes on these plots are the absolute (positive) values of changes in seismic traveltimes. Vertical axes are absolute values of changes in seismic RCs. All panels are color-coded with probability values ranged from 0 to 1. Note that the higher changes in time-lapse signals, the lower probability.

of having jointly detectable traveltime and RCs for the specific production plan, will be 30, 15, and 50 percents, using P-P, P-SV, and SH-SH, respectively. In general, the higher changes in time-lapse signals, the lower probability.

Finally, evaluating various production plans with different reservoir properties will be an effective and a quantitative forward modeling approach to determine whether or not a reservoir is a candidate for acquiring MC 4D seismic data.

SUMMARY AND CONCLUSIONS

Time-lapse cross-plots of changes in MC RCs versus changes in traveltimes due to production show a separation between saturation and pressure and may have the capacity to quantitatively estimate and discriminate dynamic reservoir properties. In addition, we propose an effective statistical approach to estimate the detectability of a known production plan using MC seismic data. Time-lapse cross plot itself, single, and joint probability detectors help us to understand the efficacy of P-SV and SH-SH seismic time lapse data along with conventional P-P time-lapse reflectivity data.

The results of applying the proposed approach on three different synthetic reservoirs, consolidated, poorly consolidated and medium consolidated sandstones, are consistent with our intuition regarding the detectability of fluids within different reservoir types. This study suggests that fluid flow detection by seismic data is significantly limited for consolidated sandstone reservoirs. However, the detection is plausible for poorly to medium consolidated reservoirs in the present of realistic seismic noise level. In these cases, conventional P-P seismic data is dominant in amplitude change compared to converted P-SV and pure SH-SH seismic data. P-P data reflects the changes in fluid saturation and pore pressure. However, the primary factor is the saturation effect. SH-SH seismic data are most sensitive to the pressure thorough traveltimes portion of pre-stack data. P-SV seismic data is the weakest detector in terms of time-lapse amplitude, but its traveltime shows an intermediate trend between P-P and SH-SH seismic data.

Our observations suggest that in a waterflooding scenario, SH-SH and P-SV reflectivity data provide valuable information, if detectable changes in pore pressure accompany changes in water saturation. In contrast, P-SV and SH-SH reflectivity data are less valuable, if changes in water saturation within the reservoir are the only or dominant production-induced effects on seismic reflectivity data.

Several conclusions can be made by changing porosity, clay content, thickness, fluid type, fluid distribution type (Patchy and uniform), and production scenario. Different quality measures for the seismic data, such as improved time resolution may make detection more quantifiable further aiding our understanding of the benefits of time lapse seismic as reservoir properties change.

In this study we select three sandstone reservoirs with 100 meter thickness. Classification techniques based on the seismic observations can be unreliable due to wavelet and tuning effects in thin reservoir units. To overcome this problem, inverted seismic parameters, e.g., AI, and SI extracted from pre-

stack seismic data for both base and monitor surveys can be employed to estimate and discriminate fluid saturation and pore pressure.

In general, as is the case for any seismic reservoir characterization study, limitations include seismic noise, thickness tuning, and stiff rocks with low porosity. In addition, repeatability in seismic data acquisition and processing, and the low density contrast between hydrocarbon and injected fluid can limit the success of any seismic time-lapse project. Depth registration for MC seismic data has not been addressed in this study and we assume that depth registration for base and monitor surveys are already performed between all components of seismic reflectivity data.

The proposed methodology to estimate and discriminate saturation and pressure is only appropriate for single layer reservoirs. In multi-layer reservoirs, the cumulative effects of individual layers may prevent us from distinguishing patterns from one another. However, statistical detectability of fluid flow proposed in this study, can be generalized for any reservoir time-lapse study under various production scenarios.

Finally, we assume that water injection into black oil reservoirs is an isothermal process. In addition, we assume that changes in fluid saturation and pore pressure cause mechanical compaction neither on the reservoir nor on the background shale. This assumption is not valid for compacting reservoirs, e.g., a chalk reservoir in North Sea. Time-lapse amplitude at the top of such reservoirs is a function of two changes, changes in overburden due to mechanical compaction and changes in the reservoir itself. Similarly, time shifts in such a reservoir are associated with both mechanical compaction of the reservoir and changes in saturation-pressure.

REFERENCES

Anderson, T., Zachariassen, E., Hoye, T., Meisingset, H.C., Otterlei, C., van Wijngaarden, A.J., Hatland, K. and Mangeroy, F., 2006. Method of conditioning the reservoir model on 3D and 4D elastic inversion data applied to a fluvial reservoir in the North Sea. Expanded Abstr., SPE/EAGE Conf., Vienna. SPE 100190.

Andersen, C.F., Grosfeld, V., Wijngaarden, A.J. and Haaland, A.N., 2009. Interactive interpretation of 4D prestack inversion data using rock physics templates, dual classification, and real-time visualization. The Leading Edge, 28: 898-906.

Angelov, P., Spetzler, J. and Wapenaar, C.P.A., 2004. Pore pressure and water saturation variations: Modification of Landrø AVO approach. Expanded Abstr., 74th Ann. Internat. SEG Mtg., Denver.

Avseth, P., Mukerji, T. and Mavko, G., 2005. Quantitative Seismic Interpretation., Cambridge University Press, Cambridge.

Batzle, M. and Wang, Z., 1992. Seismic properties of pore fluids. Geophysics, 57: 1396.

Behrens, R., Condon, P., Haworth, W., Bergeron, M., Wang, Z. and Ecker, C., 2002. 4D seismic monitoring of water flux at Bay Marchand: The practical use of 4D in an imperfect world. SPE Reserv. Eval. Engin., 5: 410.

Biot, M.A., 1956. Theory of propagation of elastic waves in a fluid-saturated porous solid, I: Low-frequency range; II: higher frequency range. J. Acoust. Soc. Am., 28: 168-191.

Blangy, J.P., 1994. AVO in transversely isotropic media. Geophysics, 59: 775-781.

Cole, S., Lumley, D., Meadows, M. and Tura, A., 2002. Pressure and saturation inversion of 4D seismic data by rock physics forward modeling. Expanded Abstr., 72nd Ann. Internat. SEG Mtg., Salt Lake City.

Cooper, M., Thorogood, E., O'Donovan, A., Kristiansen, P. and Christie, P., 1999. Foinaven active reservoir management: The time-lapse signal. Expanded Abstr., 69th Ann. Internat. SEG Mtg., Houston: 1640.

Fournier, F., Dequirez, P.Y., Macrides, C.G. and Rademakers, M., 2002. 2-D and 3-D lithostratigraphic interpretation of seismic data for characterization of the Unayzah formation in central Saudi Arabia. Geophysics, 67: 1372-1381.

Gal, D., Dvorkin, J. and Nur, A., 1998. A physical model for porosity reduction in sandstones. Geophysics, 63: 454-459.

Gassmann, F., 1951. On elasticity of porous media. Vierteljahrsschrift der Naturforschenden Ges. in Zurich. Joint Translation by Stanford University, 1998.

Han, D.H., 1986. Effects of Porosity and Clay Content on Acoustic Properties of Sandstones and Unconsolidated Sediments. Ph.D. Thesis, Stanford University, Stanford.

Killough, J.E., 1995. Ninth SPE comparative solution project: A Reexamination of Black-oil simulation. SPE Reserv. Simulat. Symp., 12-15 February 1995, San Antonio, TX: 135-147.

Landrø, M., 2001. Discrimination between pressure and fluid saturation changes from time-lapse seismic data. Geophysics, 66: 836-844.

Landrø, M., Veire, H.H., Duffaut, K. and Najjar, N., 2003. Discrimination between pressure and fluid saturation changes from marine multi-component time-lapse seismic data. Geophysics, 68: 1592-1599.

Lumley, D.E., Behrens, R.A. and Wang, Z., 1997. Assessing the technical risk of a 4D seismic project. The Leading Edge, 16, 894.

Lumley, D.E., Nunns, A.G., Delorme, G., Adeogba, A.A. and Bee, M.F., 2003. Meren field, Nigeria: A 4D seismic case study. Expanded Abstr., 73rd Ann. Internat. SEG Mtg., Dallas.

Lumley, L., Meadows, M., Cole, S. and Adams, D., 2003. Estimation of reservoir pressure and saturation by crossplot inversion of 4D seismic attributes. 73rd Ann. Internat. SEG Mtg., Dallas.

MacBeth, C., Floricich, M. and Soldo, J., 2006. Going quantitative with 4D seismic analysis. Geophys. Prosp., 54: 303-317.

Marsh, J.M., Bagley, G., Lewis, A., McGarrity, J., Nash, T., Parr, R., Saxby, I. and Whitcombe, D., 2001. The use of 4D seismic in reservoir management. Extended Abstr., 63rd EAGE Conf., Amsterdam.

Mavko, G., Mukerji, T., and Dvorkin, J., 2009, second edition, The Rock physics handbook-Tools for seismic analysis of porous media, Cambridge Univ. Press.

Mindlin, R.D., 1949. Compliance of elastic bodies in contact. Transact. ASME, A-259.

Rutleda, H., Elde, R., Wijngaarden, A.J., Helgesen, J., Buran, H. and Weisser, T., 2002. Time-lapse elastic inversion at the Oseberg field. 64th EAGE Conf., Florence.

Shahin, A., Stoffa, P.L., Tatham, R.H. and Sava, D., 2009. Multicomponent seismic time-lapse cross-plot and its applications. Expanded Abstr., 79th Ann. Internat. SEG Mtg., Houston.

Tura, A. and Lumley, D.E., 1999. Estimating pressure and saturation changes from time-lapse AVO data. Expanded Abstr., 69th Ann. Internat. SEG Mtg., Houston: 1655-1658.

Veire, H.H., Borgos, H.G. and Landrø, M, 2006. Stochastic inversion of pressure and saturation changes from time-lapse AVO data. Geophysics, 71: C81.

Walker, G., Allan, P., Trythall, R., Parr, R., Marsh, M., Kjelstadli, R., Barkved, O., Johnson, D. and Lane, S., 2006. Three case studies of progress in quantitative seismic-engineering integration. The Leading Edge, 25: 1161-1166.